A. Fathulla, B. Weiss,* and R. Stickler**

Short Fatigue Cracks in Technical pm-Mo Alloys

REFERENCE Fathulla, A., Weiss, B., and Stickler, R., **Short Fatigue Cracks in Technical pm-Mo Alloys**, *The Behaviour of Short Fatigue Cracks*, EGF Pub. 1 (Edited by K. J. Miller and E. R. de los Rios) 1986, Mechanical Engineering Publications, London, pp. 115–132.

ABSTRACT The nucleation and growth behaviour of fatigue microcracks in pm-Mo and pm-Mo-Ti-Zr alloys was investigated for room temperature cyclic loading at amplitudes slightly above the fatigue limit, and at a stress ratio of $R = -1$. In deformed Mo and recrystallized multiphase Mo-Ti-Zr-alloys the microcracks nucleated at intracrystalline sites and propagated in a transcrystalline manner. The advance of these cracks was considerably impeded by grain boundaries. In recrystallized pure Mo crack nucleation occurred in cyclic deformed regions in the vicinity of grain boundaries, followed by predominantly intercrystalline propagation. A transition from short-crack to long-crack growth behaviour – indicated by a pronounced change of the crack path and the extent of plastic deformation – could be noticed at a characteristic crack length independent of grain size. Based on these observations it is possible to differentiate several stages in fatigue crack growth behaviour, that is: (i) short-crack growth characterized by a marked reduction in growth rate when encountering microstructural features; (ii) a transition interval (with the lower bound related to the effective threshold stress intensity) over which with increasing crack length these interactions fade out while an increase in crack closure can be noticed; (iii) long crack growth which prevails beyond a certain crack length and which can be described by LEFM on the basis of the long-crack threshold stress intensity.

Introduction

The nucleation and growth behaviour of fatigue cracks is a field of considerable practical and theoretical significance. However, as pointed out in several recent surveys (e.g., (**1**)(**2**)(**3**)) discrepancies exist between the growth behaviour of the initially short fatigue cracks (SC), of length comparable with microstructural features, and of long fatigue cracks (LC) grown to macroscopic dimensions. Studies of nucleation and growth behaviour of SCs have been the subject of a considerable number of publications which revealed the complexity of the SC problem. One of the most striking features of SCs is their apparently irregular growth behaviour which may pose considerable problems for a conservative prediction of fatigue life, in particular under loading conditions near the fatigue limit (**1**)(**2**). Microcracks and SCs have been reported to grow at a much faster rate than LCs when subjected to cyclic loading at the same stress intensity range, in fact SCs may grow below the threshold stress intensity range of LCs. Consequently, several investigators have questioned the validity of LEFM concepts when applied to describe SC growth (**3**)(**4**).

The differences between SC and LC behaviour have been attributed to an inadequate continuum mechanics characterization of the crack tip stress and

* University of Vienna, Vienna, Austria.

strain fields associated with SCs, to effects of mixed mode crack propagation, to interactions with microstructural features, to differences in crack shape and extension mechanisms, and, in particular, to varying contributions of crack closure with increasing crack length (**5**)–(**8**).

In view of the lack of a general model for the description of SC behaviour, Schijve (**2**) has urged that information on SC propagation in technical alloys should be collected. The present investigation was planned in line with Schijve's stipulation to provide quantitative data on damage accumulation, microcrack nucleation, SC growth, and transition to LC growth for some technical alloys. Technically pure pm-Mo and multiphase pm-Mo-Ti-Zr alloys were selected as specimen materials because of their relatively low plasticity under room temperature test conditions, and their stable dislocation configuration and chemical stability in air at temperatures near ambient. These features should minimize some of the effects reported to influence the SC behaviour. Previous results on Mo materials (**10**)(**11**) have indicated significant effects of microstructure and pretreatment on SC growth.

For a more detailed investigation similar Mo-base materials with different microstructures were selected to study SC initiation and propagation at cyclic amplitudes slightly above the fatigue limit. Special emphasis was placed on the investigation of the transition from SC to LC growth behaviour. In addition, fatigue threshold and effective threshold values were determined. The measurements were carried out in a fatigue test system equipped with a high-resolution light microscope and video-recording systems for *in situ* observations of fatigue damage accumulation, SC propagation, and LC threshold measurements. In addition, SEM-replica techniques were used to provide information on details of the microcrack initiation processes.

Specimen material

Pure Mo and two Mo-Ti-Zr alloys produced by standard powder-metallurgical processing techniques were selected. The materials were provided either in the form of hot-rolled sheet (5 mm thickness) or as swaged bars (12 mm diameter), heat treated after hot-working to obtain either stress-relieved or recrystallized microstructures. Alloy designation, composition, and heat treatment of the specimen materials are listed in Table 1.

Information on microstructure, hardness, tensile properties, and values of the dynamic Young's modulus is compiled in Table 2. In the single phase pm-Mo, occasionally very fine particles could be detected. The Mo-Ti-Zr materials contained globular Zr-rich intracrystalline particles and a fine Ti-Mo rich precipitate along grain boundaries and on intracrystalline sites. The size of the globular particles was significantly different between the two Mo-Ti-Zr alloys.

Table 1 Material and specimen preparation data

Alloy designation	*Shape*	*Chemical composition*						*Heat treatment (°C/h)*	*Remarks*
		O (ppm)	*N (ppm)*	*C (ppm)*	*Fe (ppm)*	*H_2 (ppm)*	*Ti (%)*	*Zr (%)*	
Mo–SR	Bar (12 mm dia.)	22	5	5	20	5	—	—	Swaged and stress relieved (850/1)	This investigation
Mo–R	Bar (12 mm dia.)	20	5	8	22	5	—	—	Swaged and annealed (1400/2)	This investigation
Mo-Ti-Zr–1/R	Bar (12 mm dia.)	35	5	205	20	5	0.49	0.78	Swaged and annealed (1700/2)	This investigation
Mo-Ti-Zr–2/R	Sheet (5 mm thick)	215	5	310	22	5	0.47	0.077	Rolled and annealed (1800/1)	(**10**)

Table 2 Material properties

Alloy designation	*Microstructure*	*Grain size (μm)*	*Tensile properties* $\sigma_{0.2}$ *(MPa)*	σ_m *(MPa)*	*R.A. (%)*	*Hardness HV_{10}*	*Dyn. Young's modulus (GPa)*	*Fatigue limit, σ_{FL} (MPa) for N = 2 × 10^8, 20 kHz, 20°C*
Mo–SR (bar)	Elongated grains with equiaxed sub-grains (10 μm dia.)	300 × 60	590	590	33	228	330.5	420
Mo–R (bar)	Equiaxed recrystallized	100	318	440	4	179	331.3	360
Mo-Ti-Zr–1/R (bar)	Equiaxed recrystallized*	40	390	562	19	193	319.0	350
Mo-Ti-Zr–2/R (sheet)	Elongated recrystallized†	45/20	863	914	1	305		Not determined

* Small globular intracrystalline particles (Zr-rich) and fine intracrystalline and grain boundary particles (Mo + Ti rich).
† Coarse globular intracrystalline particles (Zr-rich) and fine intracrystalline and grain boundary particles (Mo + Ti rich).

Experimental procedures

The room-temperature tensile properties were determined at a strain rate of 0.0016/s. Standard specimens with a gauge length of 20 mm and a diameter of 3 mm were used. The values of the dynamic Young's modulus were obtained at room temperature by a resonance test procedure (**12**).

The fatigue properties were evaluated in a resonance test system operated at a frequency of approximately 20 kHz at zero mean stress ($R = -1$) at room temperature. Details of this test method have been published (**13**). In the present investigation fatigue tests at constant total-strain amplitudes were carried out between 10^6 and 10^9 loading cycles (N). From the total-strain amplitudes (assuming negligible plastic strain) the cyclic stress amplitudes were calculated by use of the appropriate values of the dynamic Young's modulus.

The geometry of the test specimens machined from the bars is shown in Fig. 1, plate-shaped specimens have been machined from the sheet metals with a cross-section of 5 mm × 20 mm, as reported earlier (**10**). It was the objective of this study to use identical specimens for the SC and the LC growth investigations. Thus, specimens with a rectangular cross-section in the gauge length were prepared from the cylindrical bars. A mild notch was machined in the mid-section of the gauge length in order to limit the area of maximum fatigue damage to a size readily scanned by a travelling microscope. For all experiments the gauge section of specimens was electropolished in order to eliminate residual stresses and microstructural damage resulting from the machining operation. The stress concentration factor of the notch was calculated to be 1.63. For calibration measurements miniature strain gauges were applied to the root of the notch, the experimentally determined stress concentration factor was found to be 1.67, in good agreement with the calculated value. All cyclic amplitudes cited in this paper refer to the measured surface strain in the root of the shallow notch. For LC measurements semi-elliptical surface notches were introduced by electro-discharge machining, these specimens were also used for the determination of closure effects by a modified compliance test technique (**14**).

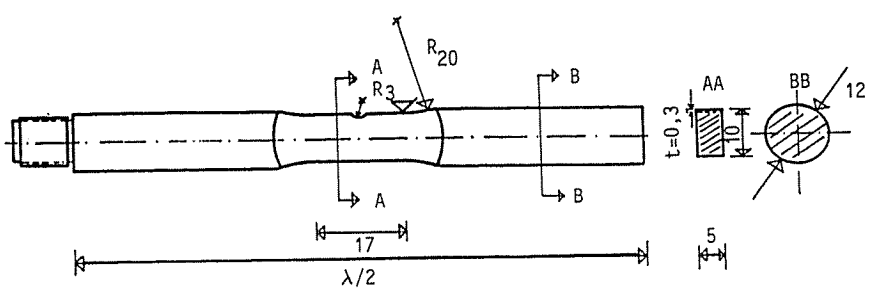

Fig 1 Test specimen for fatigue life and fatigue crack growth studies, Mo and Mo-alloys (dimensions in mm) (λ/2 = half wavelength)

The crack initiation and growth studies were performed in the same test system as described for the fatigue tests, equipped with a high-resolution travelling light microscope for the in situ observation of damage accumulation, microcrack nucleation, and fatigue crack growth up to a total length of approximately 1000 μm. The observations were recorded on video-tape synchronously with pertinent experimental information for a quantitative post-test evaluation on replay.

During the early stages of damage accumulation, of SC initiation and SC growth some specimens were subjected to a loading sequence consisting of $N = 10^4$ stress cycles (approximately 0.5 s) separated by short pauses (e.g., 1 s) during which the total notch region could be scanned and recorded by the light microscope/video system. In addition, when characteristic changes in surface topography could be noticed, plastic replicas were prepared of the entire notch surface to investigate with higher resolution the features of microcrack nucleation and initial growth. For the SEM examinations these replicas were Au-coated.

The fatigue crack growth behaviour was studied in the range of growth rates between the threshold (assumed to occur near 10^{-13} m/cycle) and 10^{-9} m/cycle for crack lengths from 2 to 1000 μm. In the present investigation the length (c) of a semi-elliptical crack on the specimen surface was measured with an accuracy of better than 2 μm. All growth experiments were carried out at cyclic stress amplitudes only slightly above the fatigue limit (experimentally determined for $N = 2 \times 10^8$) of the respective specimen materials, i.e., $\sigma_c/\sigma_{FL} = 1.07$. Crack growth ($dc/dN - c$) curves were constructed from the tangents to the measured $c - N$ curves at closely spaced points.

After completion of the crack growth experiments the electropolished region of the notch of all specimens was directly examined in the SEM. In some instances the electropolished regions were lightly etched after cyclic loading to reveal microstructure and damage zones. (Etchant: 15 g $K_3Fe(CN)_6$, 2 g NaOH dissolved in 100 ml H_2O). Subsequently some of the specimens were broken in tension to provide fracture surfaces for microfractographic evaluation and for the determination of the shape-factor of the semi-elliptical cracks at various stages of growth.

Results

Fatigue life and fatigue limit

The results of the fatigue experiments plotted as $S - N$ diagrams indicated the existence of a fatigue limit for N exceeding 2×10^8; the corresponding stress amplitudes are recorded as a fatigue failure limit in Table 2. The values of the stress amplitudes refer to the measured surface strain in the root of the shallow edge-notch of the specimens. Lack of sufficient specimen material did not permit an accurate determination of the fatigue limit of the sheet material (**10**).

Short-crack initiation and growth

Light micrographs of characteristic stages during the in situ observations of damage accumulation in a stress-relieved Mo specimen (Mo-SR) are shown in Fig. 2. As a result of the cyclic loading 7 per cent above the fatigue limit black dots were observed within individual elongated grains early in fatigue life (Fig. 2(a)). SEM-studies revealed that these dots consisted of small extrusions and intrusions associated with the subgrain structure in the stress relieved matrix. Occasionally, small particles could be detected within these deformed regions. the density of these dots increased with N until a microcrack could be observed to nucleate in one of these markings (Fig. 2(b)). This microcrack increased in length and continued to grow as a characteristic SC in crystallographic directions. Interactions with subgrain boundaries and grain boundaries can be deduced from the changes in growth direction. In this specimen the initiation of only two cracks (crack 1 and crack 2) was observed. Crack 1 apparently became non-propagating while crack 2 continued to grow and eventually linked up with crack 1.

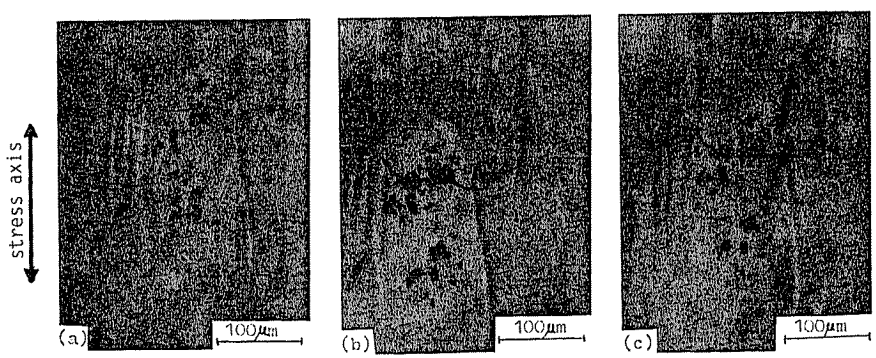

Fig 2 Damage accumulation, microcrack nucleation and SC growth in stress relieved Mo–SR, tested at $\sigma_c = 450$ MPa ($\sigma_c/\sigma_{FL} = 1.07$).
(a) $N = 6 \times 10^6$, first indication of damage, light micrograph (Point A in Fig. 3(a))
(b) $N = 5 \times 10^7$, short fatigue crack, light micrograph
(c) $N = 5,8 \times 10^7$, section of the same fatigue crack grown to a length of approximately 350 μm, light micrograph

The growth of these two SCs is plotted in the $c - N$ diagram of Fig. 3(a). The step-wise growth is a result of the retarding effects of grain boundaries, the blocking action of grain boundaries can extend for a large number of loading cycles. For example, crack 1 was held up at a grain boundary for almost 4×10^7 cycles until the slowly growing crack 2 linked-up with it. The growth data are plotted in the $dc/dN - c$ diagram in Fig. 3(b), clearly revealing a pseudo-threshold behaviour of the SC advance. It can be seen that the step-wise growth rate extends for both cracks up to a length of approximately $c = 100$ μm. this step-wise growth behaviour is considered typical for SC.

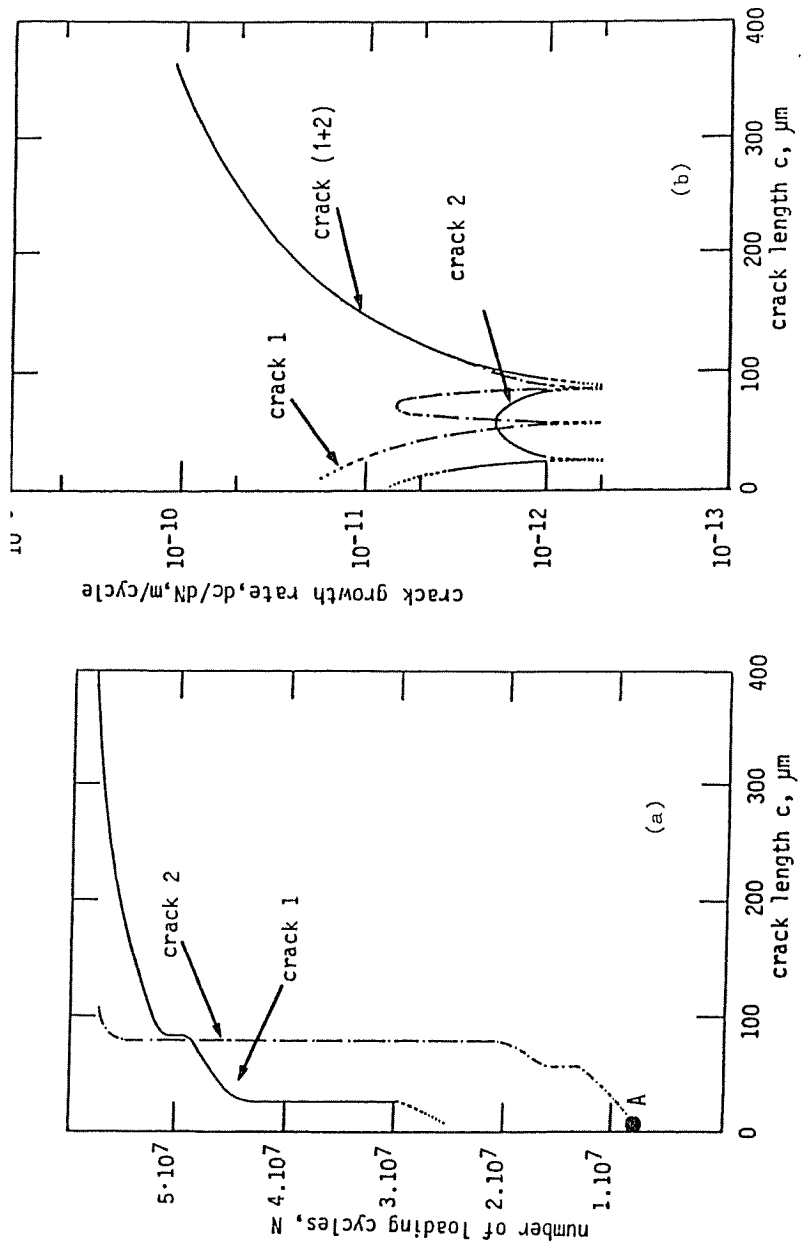

Fig 3 Growth of SCs in Mo–SR, tested at $\sigma_c = 450$ MPa ($\sigma_c/\sigma_{FL} = 1.07$).
(a) $c - N$ curves
(b) crack growth rate as function of crack length

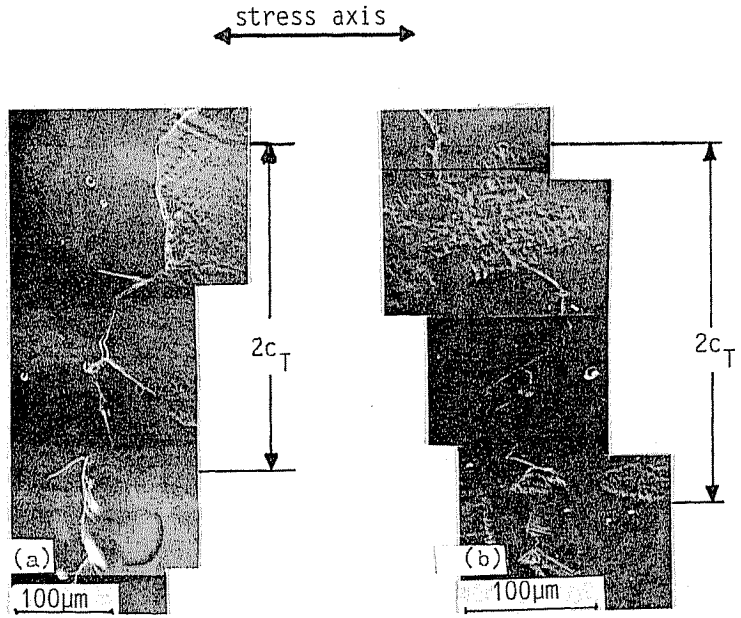

Fig 4 Comparison of crack path in recrystallized Mo and Mo-Ti-Zr specimens, SEM-micrographs of specimen surfaces.
(a) Mo–R tested at $\sigma_c = 385$ MPa ($\sigma_c/\sigma_{FL} = 1.07$) $N = 4.8 \times 10^7$ (see point A in Fig. 5)
(b) Mo-Ti-Zr–1/R tested at $\sigma_c = 375$ MPa ($\sigma_c/\sigma_{FL} = 1.07$) $N = 2.8 \times 10^7$ (see Fig. 6 and point D in Fig. 7(a))

Beyond a certain SC length the cracks assume a continuous growth behaviour characteristic of LCs. The transition from SC to LC can be deduced from micrographs such as shown in Fig. 4. The growth of the former is characterized by a crack advance along a single crystallographic plane through entire grains (typical for Stage I of fatigue crack growth); the latter exhibits an irregular transcrystalline crack path essentially normal to the stress axis (typical for Stage II of fatigue crack growth). The experiments revealed that the transition from SC to LC behaviour occurred at a characteristic crack length indicated in Fig. 4 as c_T and listed as 'transition crack length' in Table 4.

The accumulation of the fatigue damage in the recrystallized Mo (Mo–R) differs significantly from that observed in the stress-relieved material (Mo–SR). As shown in Fig. 4(a), isolated grains became gradually filled with slip markings, while neighbouring grains remained apparently unchanged. A fatigue crack nucleated along one of the boundaries between a deformed and an apparently undeformed grain; further crack growth followed, predominantly, grain boundaries without any resolvable interactions. At a crack length of approximately 300 μm indications of local plastic deformation could be seen in the vicinity of the advancing crack tip. Furthermore, a sizeable residual crack

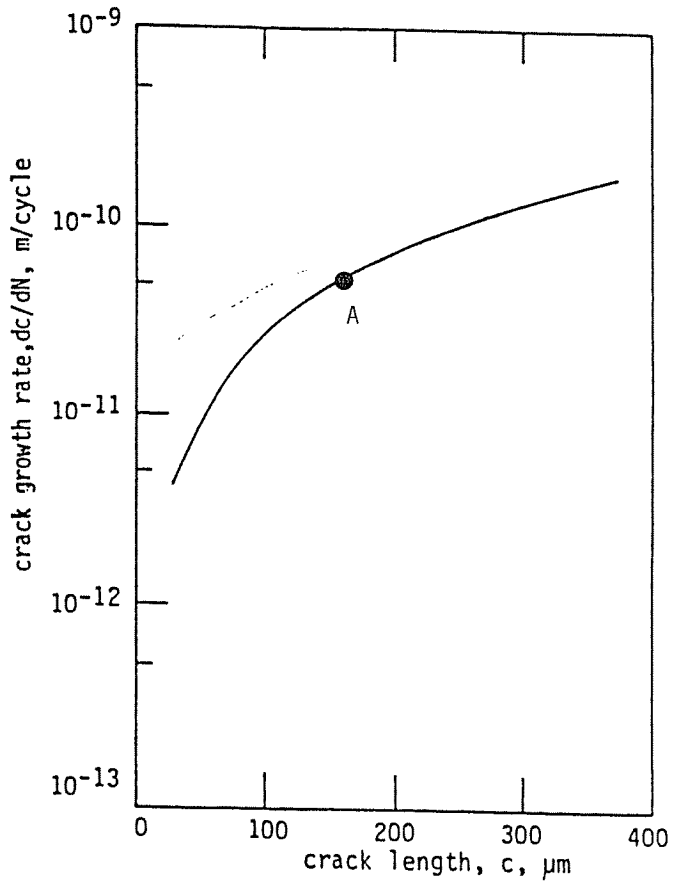

Fig 5 Crack growth rate as function of crack length for recrystallized Mo–R, tested at $\sigma_c = 385$ MPa ($\sigma_c/\sigma_{FL} = 1.07$)

opening became apparent in the unloaded specimen. The crack growth curve, Fig. 5, shows no decelerations.

In the recrystallized alloy Mo-Ti-Zr–1/R containing the finer dispersion of second phase particles the damage accumulation in the initial stages appeared similar to that in the recrystallized Mo specimen. Isolated surface grains become covered with slip markings (Fig. 6(a)). These markings, however, followed crystallographic directions and gave rise to 'embryo' microcracks (Fig. 6(b)), which joined up to form a characteristic SC (Fig. 6(c)). (The corresponding stages of these micrographs are marked on the crack growth curve in Fig. 7(a)). This SC continued to grow during further cyclic loading along single crystallographic directions through entire grains (Stage I). With increasing length the crack changed to a zig-zag crystallographic growth within

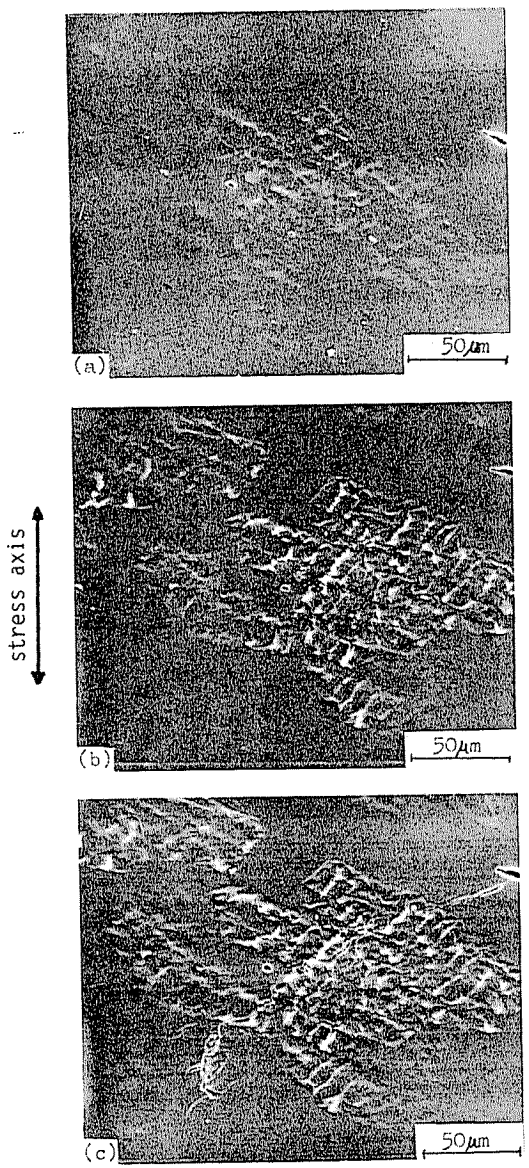

Fig 6 Damage accumulation, microcrack nucleation and SC growth in recrystallized Mo-Ti-Zr–1/R, tested at $\sigma_c = 375$ MPa ($\sigma_c/\sigma_{FL} = 1.07$) (a), (b), and (c) SEM micrographs of replicas; (d) SEM micrograph of specimen surface.
(a) $N = 6 \times 10^6$ (point A in Fig. 7(a))
(b) $N = 2 \times 10^7$ (point B in Fig 7(a))
(c) $N = 2.3 \times 10^7$ (point C in Fig. 7(a))

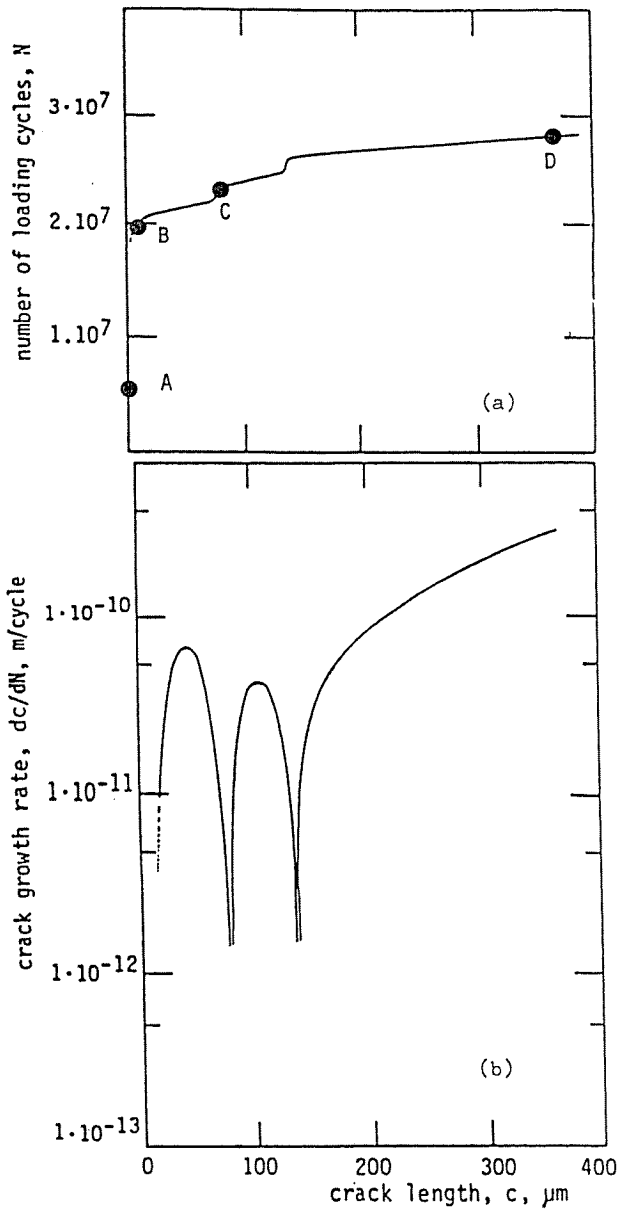

Fig 7 Growth behaviour of SCs in Mo-Ti-Zr–1/R, tested at $\sigma_c = 375$ MPa ($\sigma_c/\sigma_{FL} = 1.07$) (points A to D refer to micrographs in Figs 6 and 4(b), respectively).
(a) crack length as function of number of loading cycles
(b) crack growth rate as function of crack length

grains ('crystallographic stage II'), and finally following a transcrystalline direction normal to the stress axis ('non-crystallographic stage II'), as shown in the composite micrographs in Fig. 4(b). Slip markings which indicate plastic deformation were observed at the transition to Stage II crack growth. This change from SC to LC behaviour occurred at a crack length of approximately 300 μm. The growth curve in Fig. 7(a) shows the retarding effects of grain boundaries during the SC growth stage, less pronounced, however, than in the stress relieved Mo, (Mo–SR). In addition, the SC in the Mo-Ti-Zr alloy exhibits higher maxima of growth rate between the transient crack arrests at grain boundaries (Fig. 7(b)), although in both cases the tests were carried out at the same relative stress level (σ_c/σ_{FL}). The SC growth behaviour in this Mo-Ti-Zr alloy is very similar to that reported previously (**10**) for alloy Mo-Ti-Zr–2/R which has a different microstructure and a significantly higher tensile strength. However, the nucleation of SCs in the latter alloy occurred at large globular Zr-rich particles (up to 20 μm diameter) (Fig. 8), in contrast to the initiation within slip lines observed in the alloy Mo-Ti-Zr–1/R devoid of such large particles.

To reveal the shapes of the cracks at various stages of growth some of the specimens were broken in tension after fatigue. Fractographic examinations

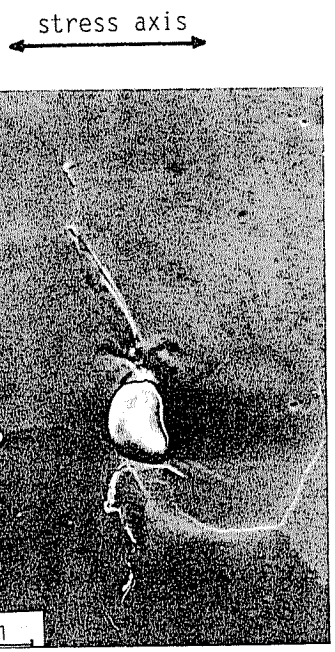

Fig 8 Fatigue damage and crack initiation at globular particle (Zr-rich) in Mo-Ti-Zr–2/R, SEM micrograph

Table 3 Mechanical properties

Alloy	*Yield strength* $\sigma_{0.2}$ *(MPa)*	*Fatigue limit* (N = 2×10^8) *(MPa), ±5%*	*Threshold stress intensity* $(MPa\sqrt{m})$, *±5%*	*Effective threshold stress intensity* $(MPa\sqrt{m})$, *±10%*
Mo–SR	590	420	10.3	7.0
Mo–R	318	360	8.5	6.6
Mo-Ti-Zr–1/R	390	350	10.1	6.3

showed that crystallographic microcracks are confined to individual surface grains, with a shape corresponding to the crack plane outlined by grain boundaries. Short cracks in the initial stages exhibited a roughly semi-circular crack front; on further SC growth the crack front changes to a semi-elliptical shape.

LC growth behaviour

The results of LC growth measurements are summarized in Table 3, in which the values of yield strength and fatigue limit are listed together with the measured threshold stress intensities and the effective threshold stress intensities calculated on the basis of the closure data.

Discussion and conclusions

The objective of this investigation was to present a detailed description of the microprocesses leading to fatigue failure. Specifically, quantitative data about the various aspects of nucleation and growth of 'short' cracks, under cyclic loading near the fatigue limit were to be determined for technical pm-Mo and multiphase Mo-Ti-Zr alloys. These alloys were selected because of their low plasticity at the test temperature, their stable dislocation substructure, and their chemical resistance to air environment near ambient temperatures, features which were thought to be essential for a minimization of the effects of plasticity at the crack tip and of corrosion products along the crack interfaces. In view of the inter-relationship between SC behaviour and the fatigue limit both properties were investigated by the use of identical specimen material, identical specimen geometry, and test procedures. The crack growth studies were carried out under cyclic loading only 7 per cent above the high-cycle fatigue failure stress limit, since earlier tests showed that in Mo alloys the fatigue limit constitutes the critical stress amplitude above which microcracks continue to grow. The experiments were designed to reveal details of the major events during the total fatigue life of a specimen, that is: (i) fatigue damage accumulation prior to microcrack formation; (ii) microcrack nucleation (length less than one grain diameter); (iii) 'short' crack development and propagation (up to a length of typically between 3 and 10 grain diameters); (iv) transition from 'short' to 'long' crack growth behaviour.

The test results reveal that under the chosen comparable test conditions the

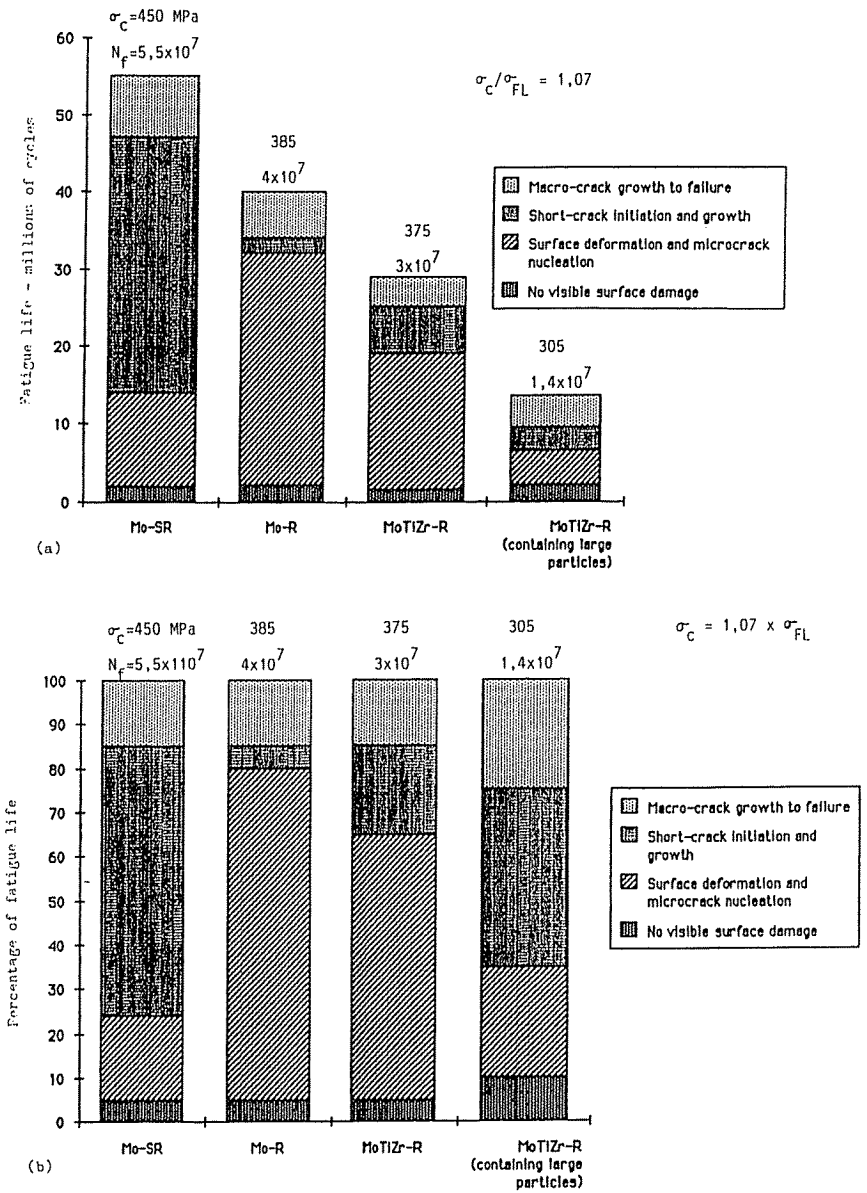

Fig 9 Damage accumulation and crack growth in specimens of Mo-alloys cycled at $\sigma_c/\sigma_{FL} = 1.07$.
(a) plotted as function of the number of loading cycles, N
(b) plotted as function of normalized fatigue life, N/N_f

characteristics of fatigue damage (e.g., damage sites, nature of damage, nucleation sites of microcracks, growth paths of 'short' cracks) as well as the fractions of fatigue life related to the various phases of fatigue, vary considerably with composition, microstructure, second phase particles, and pretreatment of the material.

The observations of fatigue damage accumulation and fatigue crack growth behaviour are summarized in Fig. 9. The relationship of surface deformation, SC initiation, and growth, as well as the transition to LC growth, are shown in the bar-graph of Fig. 9(a) as a function of the absolute number of loading cycles. In Fig. 9(b) the data are normalized by the number of cycles to failure. Both diagrams show that in all the materials, changes in surface topography could be noticed very early in fatigue life (i.e., 5–10 per cent of N_f), in spite of the low loading amplitudes. The numbers of cycles at which SC nucleation could be detected depend sensitively on the alloy and microstructure. It is possible to observe SCs very early in the stress relieved Mo; also a large fraction of fatigue life is spent on SC growth. In the recrystallized Mo, on the other hand, the deformation phase extends up to 80 per cent of the fatigue life, leaving only a short period to be divided amongst SC nucleation, SC growth, and the transition to LC growth.

The detrimental effect of large dispersoid particles is indicated by the early nucleation of SC in the high strength Mo-Ti-Zr alloy, while in a similar alloy without large particles a considerable amount of plastic deformation precedes SC formation. In all alloys investigated the period of LC growth leading to fatigue failure consumes only approximately 20 per cent of the life time, slightly more for the Mo-Ti-Zr alloy containing the large globular particles.

A significant aspect of 'short' crack behaviour is that we find a characteristic crack length associated with the transition from 'short' to 'long' crack growth. This transition is visible in a change of the crack path and/or in a marked increase in the plastic deformation associated with the advancing crack tip. The transition length appears to be a grain-size-independent parameter. The values of the measured transition length are summarized in Table 4 and compared to the grain size of the material. For the specimens with an elongated grain structure only the dimension in the growth direction (i.e., the width of the elongated grains) is considered. One interesting point is that the transition length, $2c_T$, corresponds to approximately three times the grain diameter for

Table 4 Data on transition lengths between short and long crack growth

Material	*Grain size* (μm)	$2c_T$ (μm)	$2c_T$/*grain dia.*	σ_c (*MPa*)	σ_c/σ_{FL}	*Mode fracture*
Mo–1/SR	60*	180	3	450	1.07	Transcrystalline
Mo–1/R	100	320	3.2	385	1.07	Grain boundary
Mo-Ti-Zr–1/R	40	328	10.9	375	1.07	Transcrystalline
Mo-Ti-Zr–2/R	20*	260	13	305		Transcrystalline

* In crack growth direction.

the Mo specimens, while for the two Mo-Ti-Zr alloys it exceeds 10 grain diameters, in spite of significant variations in microstructure, grain size, fatigue strength, and SC initiation.

As pointed out in previous publications **(10)(11)(14)** the transition length appears to be the characteristic critical upper bound of semi-elliptical SCs which do not affect the fatigue limit. Cracks longer than this transition length cause a gradual reduction in fatigue strength. With increasing length, crack growth occurs at consecutively lower stress amplitudes until crack advance coincides with the stress amplitudes predicted by LEFM analysis based on LC threshold considerations.

The transition length appears also to indicate the crack length beyond which a LEFM description of the crack growth process becomes applicable. However, in view of the microscopic nature of the cracks at the transition length we may assume only a negligible closure contribution; thus, we infer that the SC growth behaviour is characterized by the effective stress intensity value. A crack of length corresponding to the beginning of the SC regime should then resume growth at stress amplitudes computed from the effective threshold stress intensity. In fact, our results presented in a Kitagawa-type diagram show that the transition length corresponds closely to the crack length given by the intersection of the sloping line calculated for the value of the effective threshold stress intensity and the fatigue limit, as shown in Fig. 10. The differences between the numerical values in Table 3 and in Fig. 10 may be attributed to differences in the sensitivity of the various test methods. An interesting point realized by Fig. 10 is that the lines corresponding to the effective threshold stress intensities for pure-Mo and for the dilute Mo-Ti-Zr alloy are close together, while the fatigue limits as well as the LC threshold data differ. It follows that the values of the critical transition crack length vary to a lesser degree than the values of the crack length beyond which crack growth obeys the LC threshold relationship.

We may conclude that the growth behaviour of SCs beyond the transition length can be predicted by LEFM, provided the effective value of the threshold stress intensity is applied. Only for considerably longer cracks (in the order of 1 mm) can the growth behaviour be characterized by the conventional LC threshold stress intensity.

The observations show that the growth of SCs shorter than the transition length occurs by a glide-plane decohesion mechanism, details of which are not at present understood, but for which it may be assumed that conventional LEFM concepts are in principle not applicable. In this context the observations that residual crack opening can only be observed for cracks exceeding the transition length, at a length where measurable plastic deformation associated with the crack tip can be revealed, may be of significance.

The information accumulated in the present investigation is considered to have significant implications for advanced models of fatigue life prediction and engineering fail-safe design concepts. It should also be of relevance to guidelines for optimization of alloy processing and selection.

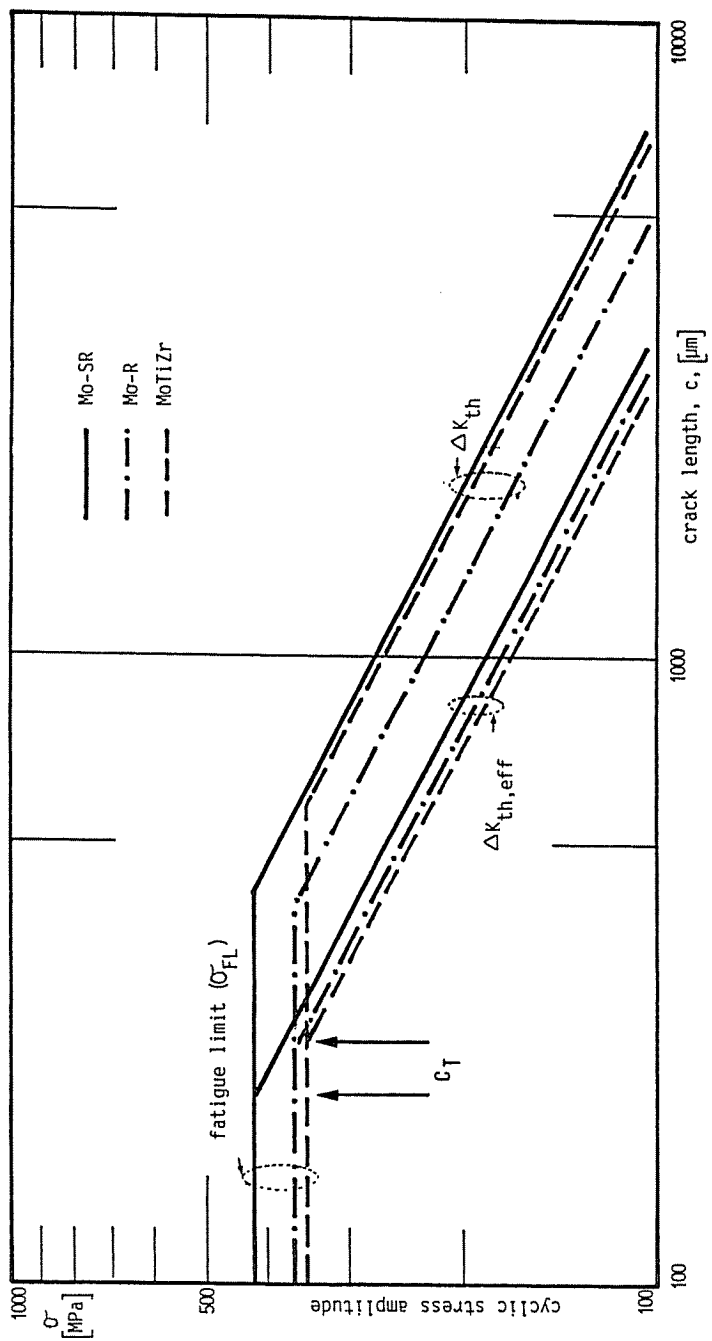

Fig 10 Effect of crack length on stress amplitude for crack growth in Mo-alloys

Acknowledgements

This investigation was supported in part by the Hochschuljubiläumsstiftung der Gemeinde Wien, Vienna, and the Metallwerk Plansee GmbH, Reutte. The authors thank in particular Mr J. Femböck of the Metallwerk Plansee GmbH for technical support of this program and for providing specimen materials with pertinent data.

References

(1) SURESH, S. and RITCHIE, R. O. (1984) Propagation of short fatigue cracks, *Int. Met. Rev.*, **29**.
(2) SCHIJVE, J. (1984) The practical and theoretical significance of small cracks, *Fatigue 84* (Edited by Beevers, J.), (EMAS, Warley), Vol. II, p. 751.
(3) MILLER, K. J. (1984) Initiation and growth rates of short fatigue cracks, *Proc. Eshelby Memorial Conf.*, Sheffield, IUTAM Conference (Cambridge University Press), pp. 473–500.
(4) KLESNIL, M., POLAK, J., and LISKUTA, P. (1984) Short crack growth close to the fatigue limit in LC-steel, *Scripta Met.*, **18**, 1231.
(5) HEUBAUM, F. and FINE, M. E. (1984) Short fatigue crack growth behavior in a HSLA-steel, *Scripta Met.*, **18**, 1235.
(6) McEVILY, A. J. and MINAKAWA, K. (1984) Crack closure and growth of short cracks and long cracks, *Scripta Met.*, **18**, 71.
(7) MINAKAWA, K. (1984) On the development of crack closure with crack advance in a steel, *Scripta Met.*, **18**, 1371.
(8) JAMES, M . N. and SMITH, G. C. (1984) Short crack behavior in steels, *Proc. ICF-6* (Edited by P. R. Rao *et al.*), New Delhi, p. 2117.
(9) RITCHIE, R. O. (1984) *Fatigue crack growth threshold concepts* (Edited by S. Suresh *et al.*), (AIME, New York), p. 555.
(10) FATHULLA, A., WEISS, B., and STICKLER, R. (1984) Initiation and propagation of short cracks, *Proc. International Spring Meeting, French Metals Society* (Edited by P. Rabbe), p. 182.
(11) FATHULLA, A., WEISS, B., STICKLER, R., and FEMBÖCK, J. (1984) The initiation and propagation of short cracks in pm-Mo and Mo-alloys, *Proc. 11th Plansee Seminar* (Edited by H. Ortner), p. 45.
(12) HESSLER, W. (1982) PhD thesis, University of Vienna.
(13) STICKLER, R. and WEISS, B. (1982) Review of the application of ultrasonic fatigue test methods for the determination of crack growth and threshold behaviour of metallic materials, *Proc. Inter. Conf. on Ultrasonic Fatigue* (Edited by J. Wells *et al.*) (AIME, New York), p. 135.
(14) BLOM, A. F., HEDLUND, A., ZHAO, W., FATHULLA, A., WEISS, B., and STICKLER, R. (1986) Short fatigue crack growth in Al 2024 and Al 7475, The Behaviour of Short Fatigue Cracks, EGF Pub. 1 (Edited by K. J. Miller and E. R. de los Rios), (Mechanical Engineering Publications, London), 37–65 (these proceedings).